2022

Electrooptic, pyroelectric and dielectric spectroscopic studies of nematic and twist bend nematic phases of achiral hockey-shaped bent-core liquid crystal

Sithara P. Sreenilayam

Neelam Yadav

Yuri Panarin

See next page for additional authors

Funder: US-Ireland Program; National Science Foundation USA

Authors
Sithara P. Sreenilayam, Neelam Yadav, Yuri Panarin, G. Shanker, and J.K. Vij

Journal of Molecular Liquids 351 (2022) 118632

Contents lists available at ScienceDirect

Journal of Molecular Liquids

journal homepage: www.elsevier.com/locate/molliq

Electrooptic, pyroelectric and dielectric spectroscopic studies of nematic and twist bend nematic phases of achiral hockey-shaped bent-core liquid crystal

Sithara P. Sreenilayam [a,b], Neelam Yadav [a], Yuri P. Panarin [a,c], G. Shanker [d], Jagdish K. Vij [a,*]

[a] Department of Electronic and Electrical Engineering, Trinity College Dublin, The University of Dublin, Dublin 2, Ireland
[b] Advanced Processing Technology Research Centre, School of Mechanical and Manufacturing Engineering, Dublin City University, Dublin 9, Ireland
[c] Department of Electrical and Electronic Engineering, Technological University of Dublin, Dublin 7, Ireland
[d] Department of Chemistry, Bangalore University, Jnana Bharathi Campus, Bangalore, India

ARTICLE INFO

Article history:
Received 16 November 2021
Revised 24 January 2022
Accepted 26 January 2022
Available online 30 January 2022

Keywords:
Twist-Bend Nematic Phase
Bent-Core Liquid Crystals
Electro-optics of Liquid Crystals
Pyroelectricity
Dielectric Spectroscopy

ABSTRACT

Experimental and theoretical investigations of the twist-bend nematic (N_{TB}) phase in liquid crystals have recently received significant attention for reasons of unusual and interesting characteristics of the N_{TB}. Though N_{TB} was predicted to exist for rigid bent-core LCs by Ivan Dozov in 2001, nevertheless it has unambiguously been proven to exist only in a few bent-core systems so far. Here the characteristics of both the nematic (N) and N_{TB} phases are investigated for a hockey shaped achiral rigid bent-core LC, called BCI, in planar and homeotropic aligned cells, using polarizing optical microscopy, electro-optics, pyroelectricity and wide band dielectric spectroscopy. Spontaneous polarization measured for a bias field of 2.2 V/μm of a chiral domain using the pyroelectric effect is found to be only ~5 nC/cm^2. A measurement of the spontaneous polarization using pyroelectricity in general is unaffected by the sample's dc conductivity except when its conductance dominates the admittance. As helix of N_{TB} is partially unwound by the field, results lead to the identification of N_{TB} as polar and chiral. The first and the second harmonics of the applied field are observed of higher amplitudes in N_{TB} and N phases, respectively. The hockey-shaped bent-core system exhibits a large negative dielectric anisotropy over a wide range of temperatures than observed for any other compound so far. The large negative dielectric anisotropy is the highly desirable characteristic parameter of the N_{TB} for exploring the field induced phases at relatively lower field strengths. The orientational order parameter characteristically jumps at the N-N_{TB} transition temperature. The complex dielectric permittivity is measured as a function of frequency in the range 1 Hz to 10 MHz, the analysis of results reveales two collective modes in the dielectric spectra. Amplitude of the lower frequency mode is much higher than of higher frequency, former is assigned to the hydrodynamic mode $\boldsymbol{q} = q_z\hat{\boldsymbol{z}}$ with z-dependent rotation of the heloconical director $\hat{\boldsymbol{n}}(\boldsymbol{r})$, this in turn involves compression and dilation of the pseudo-layers. The higher frequency mode corresponds to fluctuations of the tilt director and closer to the transition temperature, it exhibits a typical soft mode characteristic feature.

1. Introduction

In the last decade, significant attention of the liquid crystals community is focused on to investigating systems that exhibit nematic-nematic phase transitions, such as N-N_{TB} and N to Ferroelectric Nematic (N_F). Prior to these observations, the phase transitions in nematic phase had rarely been observed. At the N to N_{TB} transition, the higher temperature nematic mesophase was found to resemble mostly the ordinary nematic phase (N), whereas the lower temperature enantiomorphic phase though proven nematic was found to have different characteristics and it was initially denoted as the Nx phase [1]. This phase is now identified as the 'twist bend nematic' N_{TB} [2,3], this was the first example of the chiral symmetry breaking in a fluid state, where achiral molecules lead to the spontaneous formation of chiral domains of opposite handedness. In each chiral domain, the molecules spiral around the helical (optic) axis either left or right-handed and form a helicoid with a helical pitch of approximately 10 nm [2,3]. The N_{TB} phase was predicted to exist for both chiral and achiral bent-core systems by Meyer [4] and Dozov [5] and confirmed through computer simulations by Memmer [6]. The N_{TB} phase has been discov-

* Corresponding author.
E-mail address: jvij@tcd.ie (J.K. Vij).

https://doi.org/10.1016/j.molliq.2022.118632
0167-7322/

ered in one other bent-core liquid crystal [7]. However this molecule has a bent-core only in the center, in addition it has two rod-like cyano-biphenyl terminals separated by spacers from the two ends of the bent-core. This molecule is diferent in shape than the hockey-shaped molecule and is called a trimer. In a number of bimesogens, two oppositely handed chiral domains in a thin planar-aligned cell were observed first by Panov et al. [8,9]. These domains were later confirmed by Nuclear Magnetic Resonance (NMR) spectroscopy [10]. Hierarchy of various structures of N_{TB} for different length scales are shown in Fig. 1 (a to d). The helical pitch of N_{TB} determined using freeze-fracture transmission electron microscope (FFTEM) technique ranges from 8 to 12 nm (Fig. 1d), magnitude of the pitch and its structure were confirmed using resonant X-ray scattering techniques [11,12]. An additional important characteristic of N_{TB} is the establishment of a hierarchy of self-deformation patterns that extend in scale from the nanometer to the micrometer [13]. Though this is not yet fully established. The molecular deformations lead to the display of striped textures, periodicity of which is determined by the liquid crystal (LC) confining sample geometry. In homogeneously planar aligned cells, periodicity of the stripes is found exactly two times the confining cell gap and is independent of temperature. In twisted cells, however periodicity of stripes was found lower than two times the cell-spacing and it was also dependent on temperature [14]. In each of the two chiral domains, the helical structure of the right or the left-handed winding exists (1e), the molecular director forms an angle (θ) with the helical axis, magnitude of the heliconical angle lies between zero and $\pi/2$ rad [2,3] just like in SmC* (Fig. 1f) with two exceptions: (a) molecules in SmC* are chiral and (b) helical pitch of SmC* lies in the visible wavelength range. In cholesteric N* phases (Fig. 1g), the constituent molecules are also chiral, however while continually changing their directions by a small angle, but these are always oriented perpendicularly to the helical axis. The helical pitch in the cholesteric phase lies in the visible wavelength region. The N_{TB} phase is found to exhibit an ultra-fast switching time of 0.7 μs arising from flexoelectric effect [15]. Fast switching offers enormous potential in having electro-optic devices fabricated on the phenomena of flexoelectricity.

In this paper, we report results obtained from experimental investigations of N and N_{TB} phases of a rigid bent-core hockey shaped LC (called BCI) using planar and homeotropically aligned cells. The LC sample cells are studied using polarizing optical microscopy (POM), electro-optics, pyroelectricity and dielectric spectroscopy. Temperature dependence of the orientational order parameter *S* with respect to the optical axis (director) is determined for both N_{TB} and N phases from measurements of the birefringence at a visible wavelength of light. The birefringence observed in the N phase is extrapolated to lower temperatures using the Haller method [16]. For a bias field of 2.2 V/μm, the spontaneous polarization, Ps, in N_{TB} phase is found as ~ 5 nC/cm^2. This result confirms the polar characteristic and the chirality of N_{TB}. Ps measured using the pyroelectric technique is unaffected by the material's dc conductivity unlike results obtained using other techniques. Dielectric anisotropy in the entire temperature range of N and N_{TB} phases is calculated from the results of the complex permittivity measurements made for both planar and homeotropically aligned cells. The dielectric anisotropy is 'negative', the permittivity normal to the long molecular axis is greater than along it. The dielectric spectra in the investigated frequency range 1 Hz – 10 MHz show two collective relaxation modes in N_{TB}. The molecular modes are not observed in the frequency window of the experiment.

2. Materials and methods

The two arms of a rigid bent-core compound, one longer than the other, are terminated by symmetric alkoxy chains having six carbon atoms in each chain (n = 6) (Fig. 2a). Planar and homeotropic alignments are achieved by coating indium tin oxide (ITO) glass substrates with RN1175 (Nissan Chemicals, Japan) and polymer solution AL60702 (JSR, Korea), respectively. Temperature of the cell is controlled by a Eurotherm 2604 temperature controller. The LC cell is heated initially to a temperature of the isotropic (Iso) state of the material, it is then filled by a liquid crystalline material in isotropic phase by capillary action. A cell spacing between the two electrodes is controlled by having different thicknesses of

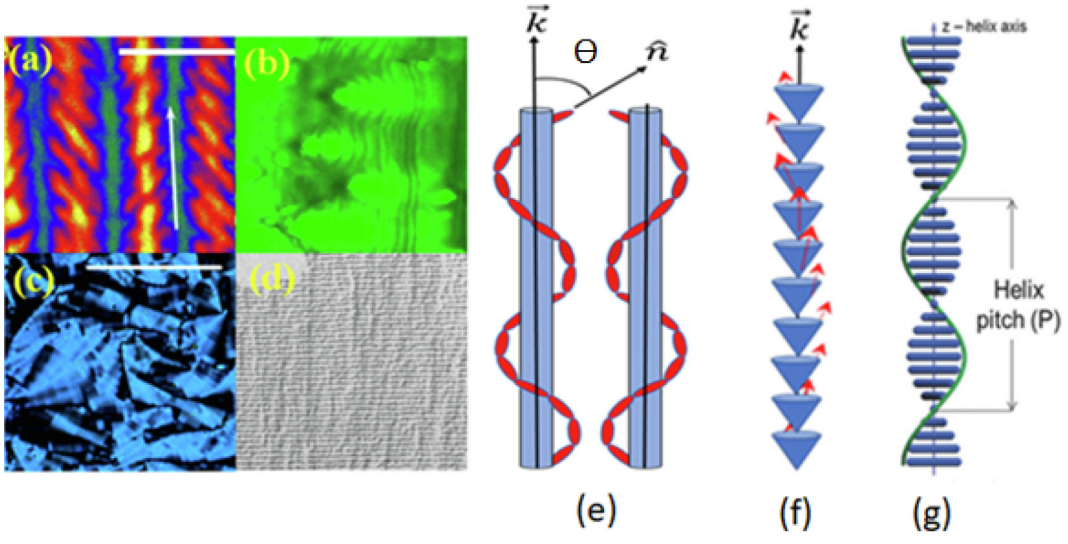

Fig. 1. A hierarchy of the structures of N_{TB} (details under experimentation) (a) Fluorescent Confocal Microscopy – periodicity the stripes = 2 times the cell-thickness, length of the white bar in (a) is 4 μm,the slanting structures in the middle of each stripe correspond to the rope like structure in POM. These are suggested to arise from the special packing arrangement of the molecules, see Fig. 3e. (b) structures that appear to be fish like are observed in confocal microscopy at visible wavelengths, striations normal to the rubbing direction indicate psuedo-layers structure (c) chiral domains of the opposite handedness (right and left-handed) Length of the white bar in (c): 10 μm (d) Freeze-Fracture TEM, pitch = 8 nm (e) twist bend nematic structure at the nanometer scale (f) SmC* in the absence of the external field, the arrows represent molecular directors that form the helix (g) the cholesteric phase. The helical pitch in (f) and (g) lies in the range of visible wavelengths.

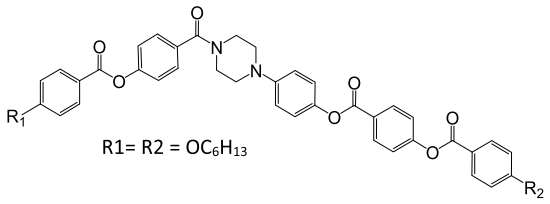

(a) **Cr** 129°C **Col** 150°C **N$_{TB}$** 166°C **N** 190°C **Iso**

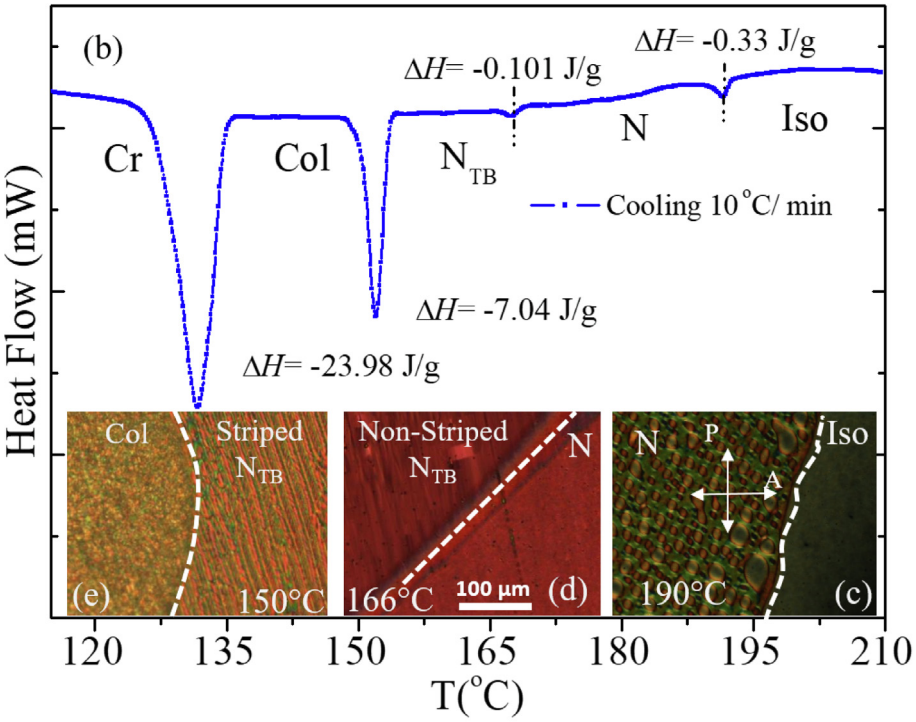

Fig. 2. (a) Molecular structure, phase sequence and the phase transition temperatures [T (°C)] of an achiral bent-core LC material BCI obtained using DSC. The phase transition temperatures are obtained in quasi-equilibrium conditions under cooling at a rate of ~ 10 °C min-1 by DSC. POM is studied at a temperature step of 1 °C min^{-1}. Abbreviations used here are as follows: Iso → Isotropic, N → Nematic, N_{TB} → Twist Bend Nematic, Col → Columnar and Cr → the solid crystalline state. (b) These mesophases are labelled in the DSC scan. Superimposed on these are textures at the transition temperatures of (c) 190 °C (Iso-N), (d) 166 °C (N-N_{TB}) and (e) 150 °C (N_{TB}-Col) in a temperature gradient cell recorded using a planar aligned cell. Broken white lines in Figures (c to e) indicate the phase transitions between two consecutive phases.

Mylar spacers. The cell spacing is measured using optical interference technique developed in the laboratory. Optical textures are recorded under crossed polarizers in both N and N_{TB} phases using Olympus BX 52 Polarizing Optical Microscope (POM). The LC cell is mounted in a hot stage, the latter is fixed on to the rotating table of POM. A digital camera records the transmitted light of the POM. The light is sensed by Hamamatsu C6386 photo-diode. The camera records textures at different temperatures in the N and N_{TB} phases under conditions of confinement the LC cell. Prior to initiating measurements of birefringence, the quality of alignment in the LC cell is confirmed using POM. Planar and homeotropically aligned cells are also fabricated using the two ITO coated substrates, each having a low sheet resistance of 20 Ω/□. The real and the imaginary parts of the complex dielectric permittivity of the sample in the cell are measured in planar aligned cells using both gold-plated and ITO electrodes in a frequency range of 1 Hz to 10 MHz. Cells are cooled slowly with a temperature step of 0.5 °C. A comparison of the results using planar aligned cells with gold-coated electrodes and low ITO sheet resistance shows that the parasitic peak arising from the finite ITO sheet resistance in series with the LC sample's capacitance is shifted to frequencies beyond the frequency window of these experiments.

3. Results

3.1. Polarizing optical microscopy (POM) and the differential Scanning calorimetry (DSC)

The POM and DSC studies of this material in a LC cell exhibit the following phase sequences: Iso 190 °C N 166 °C N_{TB} 150 °C Col 129 °C Cr under cooling from the isotropic phase and Cr 166 °C N 191 °C Iso on heating from the crystalline (Cr) state [15]. Four phase transitions are observed from DSC scans under cooling at a rate of 10 °C per minute. These records show the occurrence of two strong at 150 °C and 129 °C and the two weak first-order phase transitions at 166 °C and 191 °C (Fig. 2b). Since both N_{TB} and the Col phases are observed only under cooling, the LC material is monotropic. A homologous series of the compound with different number of carbon atoms in alkoxy group were studied by Schröder et al. [17] who identified the lower temperature nematic phase as another 'columnar'.

The Schröder et al. compound was studied initially by Chen et al. [18] who identified the low temperature phase as N_{TB} instead of another columnar as had previously been suggested by Schröder et al. [17]. The helical pitch of 14 nm using the freeze fracture

Transmission Electron Microscopy (FFTEM) was reported by Chen et and who also observed two oppositely handed chiral domains in a planar-aligned cell and found that the electroclinic effect in itself was weak [18]. Textures of the cell are recorded under cooling from the Iso to a series of LC mesophases in the absence of an external electric field. Studies of a planar aligned LC cell show that the phase identified at 190 °C is nematic (Fig. 2c). A uniform texture in nematic phase changes to nonuniform one, yielding N-N_{TB} (non-striped) phase transition at a temperature of 166 °C (Fig. 2d), whereas the non-striped phase persists only over a very narrow range of temperature of 1.5 °C. On further cooling, the observation is followed by the emergence of striped N_{TB}, the phase continues to exist over an extended range of temperatures of 15 °C. On further cooling, the phase transition from striped N_{TB} to Col is observed at a temperature of 150 °C (Fig. 2e). Textures of the sample in a planar-aligned cell of the cell-spacing 15 μm are recorded and shown in Fig. 3. Here the LC sample cell is adjusted in a manner that the rubbing directions ***R*** on the top and the bottom substrates are adjusted to overlap with each other. The cell with the overlapped ***R*** makes an angle α = 22.5° with the polarizer direction, ***P***. The stripes emerge spontaneously parallel to the rubbing direction with a periodicity of exactly two times the LC cell spacing, and independent of temperature within the N_{TB}. This is an important characteristic feature of the N_{TB}, deformations of molecules may arise from the tilt of the molecular director with respect to the optical axis (Fig. 2e and 3c). A detailed subsequent investigation using POM showed that the predominant structure in the middle of each stripe is 'rope-like' (Fig. 3c) as was also confirmed by Fluorescent Confocal Polarizing Microscopy (FCPM) carried out on bimesogens [19] and is shown in Fig. 1 (a). Left and the right-handed twisted rope like structures were also observed by Agra-Kooijman et al. in bimesogen CBC7CB by OPM [20]. Here the rope-like structure is shown to reflect the twisting and bending of the molecules as revealed by scanning the polymerized template of CBC7CB bimesogen using Scanning Electron Microscope (SEM) shown in Fig. 3e.

DSC scans under cooling reveal that the transition enthalpy (ΔH) of the N-N_{TB} transition is extremely low ~ 0.1 J/g (Fig. 2b) and the phase transition is weakly first order. As the LC cell is cooled further to a temperature of 153 °C, a mosaic-like texture is recorded in a planar aligned cell (Fig. 3d). A large change in the enthalpy (ΔH) of 7.04 J/g for the N_{TB} – Col phase transition (Fig. 2b) corresponding to a strong first order transition is recorded. The mosaic-like texture of a planar aligned cell for the Col phase at a temperature of 153 °C is a periodic stripe pattern (Fig. 3d). The X-ray Diffraction (XRD) study of the compound in Col phase exhibits two peaks, q ~ 0.205 $Å^{-1}$ and q ~ 0.281 $Å^{-1}$, corresponding to the rectangular columnar lattice with parameters, a ~ 42.5 Å and b ~ 44.5 Å [17].

3.2. The polarization measurements

The spontaneous polarization is a major characteristic parameter of the ferroelectric and polar LC phases of a liquid crystal. Different techniques for measuring the spontaneous polarization are described in the literature. A commonly used technique is based on measuring the repolarization current that flows through the LC cell on applying a triangular waveform [22]. Another method

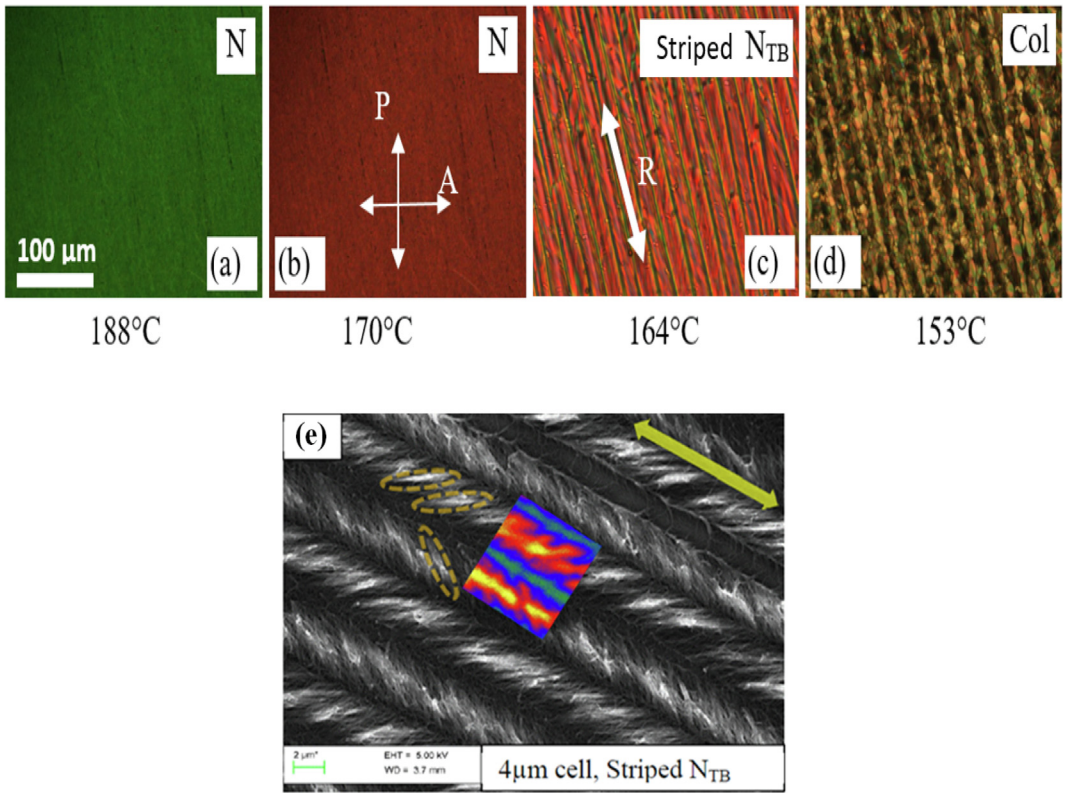

Fig. 3. The POM textures of mesophases in a 15 μm planar aligned cell. The phases indicated are: (a) N at 188 °C, (b) N at 170 °C, (c) N_{TB} at 164 °C (2 °C below the N -N_{TB} transition temperature) and of (d) the Columnar phase at 153 °C and (e) Imaging of the polymerized template of N_{TB} phase in a mixture of CBC7CB and 5 CB (designed for reducing N-N_{TB} transition temperature) in a planar-aligned cell (cell-spacing 4 μm) using Scanning Electron Microscope (SEM). The left and the right handed molecular packing with twist and bend of the molecules in neighbouring layers is revealed by SEM imaging. The yellow twisted helices seen in Fig. 3(e) correspond to the rope-like structure observed in Fig. 3(c). The procedure of obtaining SEM images is detailed by Panov et al. [21]. Figure 3(e) is reproduced with permission from the authors. The rope like structure obtained by Focal Conic Polarizing Microscopy (FCPM) [19] on a LC sample cell under similar conditions is overlapped on to the SEM polymer template imaging of the N_{TB} structure. The length of the bar shown (in green colour) in Figure 3e is 2 μm.

is based on integrating the switching current arising from the response of the LC cell to the applied square-wave voltage waveform by a capacitor [23]. Both techniques allow for the measurements of dynamical properties (switching time) and of the rotational viscosity of LC phases. Helices such as in SmC*, B2 ($SmC_{S/A}P_{F/A}$) and SmAP polar/helical phases are easily unwound by electric field. As a result these are found to exhibit reasonably large values of the spontaneous polarization and low viscosity. These are called 'soft systems'. However on the contrary, the helical structure such as in cybotactic nematics, twist-bent nematic (N_{TB}) cannot be easily unwound by the electric field. These are described as 'hard systems'. A commonly available technique for measuring the spontaneous polarization may lead to spurious results of P_S in hard systems resulting from a low magnitude of Ps and large dc conductivity which is difficult to eliminate. Hence we use pyroelectric technique [24] for measuring Ps in a polar/chiral phase where the total polarization $P_S(T,V)$ (T is the temperature and V is the applied voltage) gives rise to the pyroelectric coefficient $\gamma(T) = dPs/dT$. On integrating over a range of temperatures, P $s(T)$ becomes $\int_T^{Tc} \gamma(T)dT$ [24], where T_C is the N-N_{TB} phase transition temperature. A temperature change of dT occurs from a light source of constant intensity modulated and incident on to the sample's cell at a fixed frequency.

Since the magnitude of pyroelectric signal in most systems is extremely low, a lock-in amplifier (SR830) triggered by reference signal derived from the signal that modulates beam of light from the source is used. However, we need to calibrate the pyroelectric coefficient dPs/dT, i.e. as to what value of dT leads to a known change in dP_S. A change in the temperature of a system depends on several factors: absorption of light by the cell electrodes, cell design, LC sample and its heat capacity, modulation frequency and the intensity of the source of light. A comparison of the pyroelectric signal from the sample's cell with that arising from a standard material of known P_S are used for calibration purposes. We use a conventional FLC (FELIX-18) mixture with a pre-determined temperature dependence of the spontaneous polarization as before [25]. The latter is obtained using current reversal technique and a planar-aligned cell [22,23]. The LC cells used in both experiments must be of the same design. Commercial parallel aligned LC cells (EHC Co. Japan KSPR-09,) of cell-spacing of 9 μm and measured area of electrodes 0.5 cm^2 are used in the experiments. The pyroelectric response and consequently the spontaneous polarization depends on the dc applied electric field (voltage/cell spacing) and frequency at which the beam of light is modulated. For zero value of the electric field, the pyroelectric response is zero as would normally be expected from undistorted helical structure. A distortion in the structure of N_{TB} increases with increase in the field applied across the cell. The maximum signal-to-noise ratio is reached for a field of 2.2 V/μm applied across a planar-aligned cell. For fields higher than 2.2 V/μm, the output drops and electrical noise increases gradually. This will be discussed later.

It is important to select the optimum chopper's frequency for modulating the incident beam of light that yields a maximum value of the pyroelectric signal. Fig. 4 shows the frequency dependence of the pyroelectric signal measured at a temperature of 150 ^{O}C in the N_{TB} phase.

Magnitude of the pyroelectric signal is found strongly frequency dependent but it plateaus at modulating frequencies of between 20 and 30 Hz and decreases with an increase in frequency. In the narrow range of frequencies for which the signal plateaus, we select the modulation frequency of 20 Hz for the experiment. Fig. 5 shows a temperature dependence of the pyroelectric signal Vp in μV using a planar aligned cell, where the calculated macroscopic spontaneous polarization P_S using a cell with the spacing of 9 μm is also plotted as a function of frequency. In our study, we use quasi-commercial FLC mixture FELIX-18, this gives Ps = 1.35 nC/cm^2 for

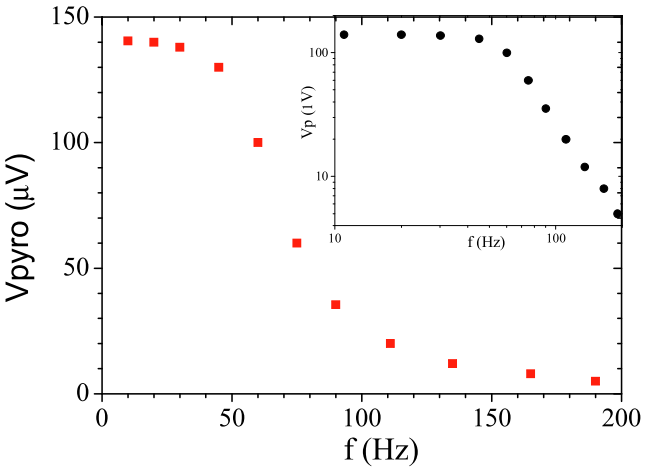

Fig. 4. Frequency dependence of the pyroelectric response measured using a commercial 9 μm thick cell (KSPR-09) at a temperature of 150 °C in N_{TB} for applied dc voltage of 20 V. Inset is the Bode plot of Vp vs. f (both plotted on the log–log scale).

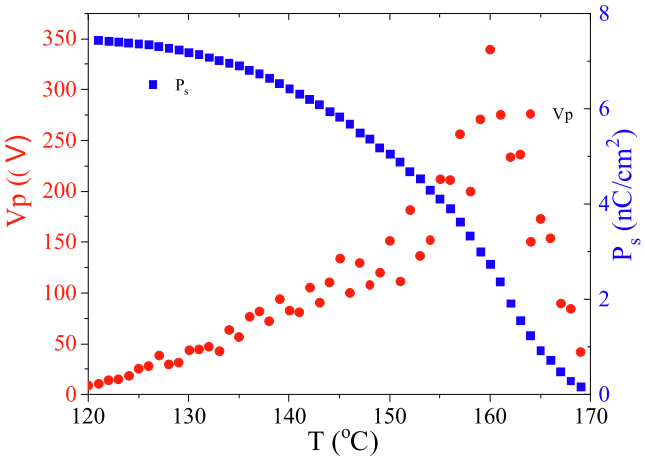

Fig. 5. Temperature dependence of the pyroelectric response Vp in μV (red filled circles) and the corresponding macroscopic polarization P_S (■ squares in blue) using a planar aligned cell on temperature, spacing between the cell electrodes is 9 μm, 20 V_{dc} is applied voltage across the cell. Frequency of the modulating signal = 20 Hz. The sample is cooled slowly at the rate of 1 °C per 5 min. The temperature dependence of Ps shown in blue follows the power law equation in temperature.

Vp = 50 V. It should be noted that the pyroelectric signal in general is noisy due to the molecular fluctuations in the nematic phase.

The pyroelectric coefficient shows a peak at a temperature of 160 °C in N_{TB} for E = 2.2 V/μm, the signal decreases gradually under cooling. The pyroelectric signal increases linearly initially with applied field. However when the applied field is increased beyond 2.2 V/μm, the pyroelectric signal slowly drops to zero. The output is finally buried in electrical noise. This observation can have two plausible explanations. Firstly the field induced N_{TB} transits to apolar splay-bend for a particular field strength, secondly the dc conductivity suddenly increases for a particular field strength. The latter is an unlikely scenario due to the fact that Ps using the pyroelectricity should normally be independent of the ionic conductivity. A drop in the pyroelectric signal for a particular strength of the field accords with a decrease in the dielectric relaxation frequency with the bias field observed for the same compound [26]. A marked increase in the birefringence for the field induced N_{TB} changing to the splay-bend (N_{SB}) in bimesogen CBC7CB [27].

3.3. The Electro-Optic response

The electro-optic response relates to measuring the output of the cell for the (a) first, and (b) second harmonics of the signal applied across a planar aligned cell. The cell inserted between the crossed polarizers is rotated in such a manner that the overlapped ***R*** of the cell substrates makes an angle of 22.5° with the polarizer direction ***P***. In this configuration, the first harmonic of electro-optical response is a result of the polar electrical interaction. However, for some systems, (e.g. SmAP and nematics), the polar interaction will lead to almost zero output for the first harmonic but finite output for the second harmonic, since the two oppositely switched states in a nematic or SmA phase are optically equivalent.

The electrical signal from the photodiode that monitors the transmitted intensity of the the POM is fed to the input of a lock-in amplifier (SR830), here the trigger/sync signal of the lock-in is derived from the signal applied across the cell. A frequency of 120 Hz is selected for the applied signal, as the lock-in amplifier for signals at fundamental and second harmonics is suitable for measurements. Frequency of the applied waveform is chosen not to coincide with the integral multiple of mains frequency of 50 Hz, this avoids interference to the electro-optic output from the noise pick-up from the mains frequency. Fig. 6 shows a plot of the temperature dependence of the first and the second harmonic electro-optical response signals for a sinusoidal signal of amplitude 5 V applied across the cell at a frequency of 120 Hz.

The planar aligned LC sample gives output for the first and the second harmonics in the electro-optic output of the applied input. We note that the first harmonic is dominant in N_{TB} but is almost zero in the N phase whereas the signal for second harmonic is dominant in the N phase. These results confirm that due to the dominant output of the first harmonic in N_{TB} , the phase is polar and chiral. The N phase gives output that is dominant only for the second harmonic for a reason that the two up and down states of the molecule are equivalent in this phase.

3.4. The order parameter determined from measurements of the temperature dependence of birefringence

The orientational order parameter, S, is obtained from measurements of the birefringence, Δn, of a planar aligned cell in the N and N_{TB} phases of BCI reported in [15]. The anisotropy in refractive index is expressed in terms of the birefringence. S at a particular temperature is determined from the ratio of Δn measured for that temperature to the extrapolated birefringence Δn_0 for zero degree K ; $S = \Delta n/\Delta n_0$. S is calculated from the birefringence data and is plotted in Figure 7. Measurement of the birefringence and its correction using Cauchy equation is given below. A planar aligned cell is used in the birefringence Δn experiments. To measure the birefringence, the transmittance spectra from the LC sample cell are recorded while keeping the angle between the ***R*** and the polarizer ***P*** directions, $\alpha = 45°$.

The transmitted light at wavelength λ from the sample cell inserted between the crossed polarizers as a function of the birefringence is given by:

$$T = A\sin^2\left(\frac{\pi\Delta n_{eff}d}{\lambda}\right) + B \quad (1)$$

A is the scaling factor, Δn_{eff} is the effective birefringence of the sample, d is the electrodes cell spacing and B is the offset signal. The transmittance spectra as a function of the wavelength are fitted to Eqn. 1. The wavelength dependence of Δn is expressed by an extended Cauchy equation using the procedure suggested first by Panarina et al. [28]

$$\Delta n_{eff}(\lambda) = k_{eff}\left(\frac{\lambda^2\lambda^{*2}}{\lambda^2 - \lambda^{*2}}\right) \quad (2)$$

k_{eff} and λ^* are the parameters of the fit of the experimental data of Δn to equation (2) for a few selected temperatures. On assuming λ^* constant over an entire range of temperatures, values of Δn are calculated for other temperatures.

The measured Δn (T) in the high temperature N-phase is fitted to the Haller equation [16],

$$\Delta n(T) = \Delta n_0\left(1 - \frac{T}{T^*}\right)^{\beta} \quad (3)$$

T is the absolute temperature. Constants of the fit are: $T^* \cong 188$ °C and $\beta \cong 0.2$. Temperature T^* corresponds to the first order Iso-N phase transition temperature. Δn is the birefringence and Δn_o is the birefringence obtained by extrapolating Δn from the high temperature N phase to absolute zero degree temperature (i.e. $T = 0$ K), where the extrapolated order parameter S reaches unity. For $S = 1$, all of the molecules are parallel to each other, i.e. in the limit, $[\lim_{T\to 0}[\log(\Delta n)] = \log \Delta n_0$. The function $\log(\Delta n)$ is linearly related to the logarithm of the reduced temperature $[(T^*\text{-}T)/T^*]$. This is valid for the data points slightly removed from the Iso-N transition temperature (T^*) which satisfy equation (3). Here $\Delta n_0 = 0.677$ is obtained from the extrapolation of the Haller fit from higher temperatures. In the N and N_{TB} phases, the orientational order of the bent-core molecules though relatively low, nevertheless S is strongly temperature dependent in the N phase. We observe a large jump in S of 0.36 at the Iso-N transition, this is followed by a drop in S at the N-N_{TB} transition temperature. This is caused by a tilt of the molecular directors from the helical axis. For temperatures lying within the non-striped N_{TB} phase, S reaches ~ 0.499 at 167 °C from a low value of 0.364 at 189 °C. At the Iso-Nematic transition S jumps from zero to 0.36, a strong first order In this compound, small jumps in S and Δn are observed at the N to non-striped N_{TB} and at the non-striped to striped N_{TB} transition temperatures. Magnitude of S and its temperature dependence in N and N_{TB} phases agree closely with the results for CBC7CB bimesogen using the Raman scattering experiments [29].

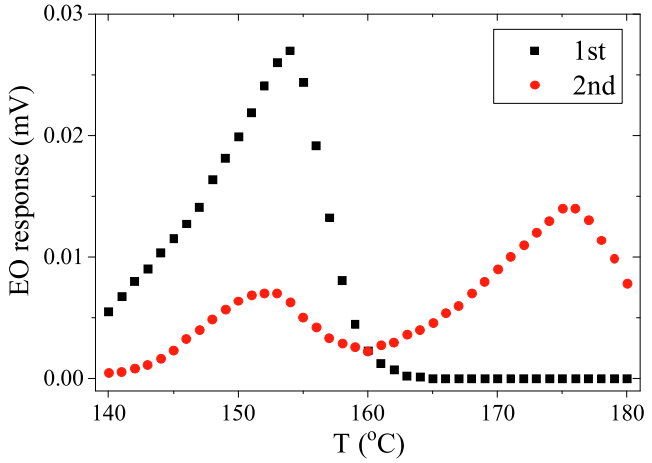

Fig. 6. Temperature dependence of the 1st and 2nd harmonic electro-optical signals for the 5 V sinusoidal signal at a frequency of 120 Hz applied across a planar-aligned cell. The N-N_{TB} transition temperature has shifted and here it is 161 °C.

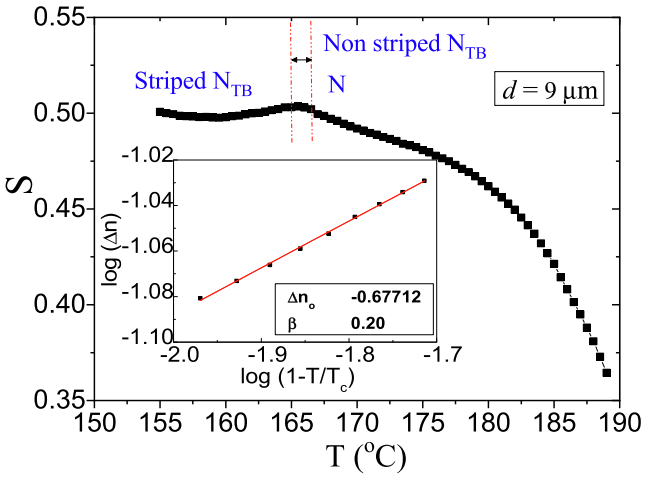

Fig. 7. The orientational order parameter, *S*, for N and N_{TB} phases as a function of temperature *T* in the absence of the external electric field. The Inset shows a plot of the temperature-dependent experimental Δn (■). The red line shows a fit of the experimental data to the Haller's equation. The rubbing direction, ***R***, of a planar aligned cell, of cell-spacing 9 μm, is fixed at an angle of 45° to the polarizer axis, ***P***.

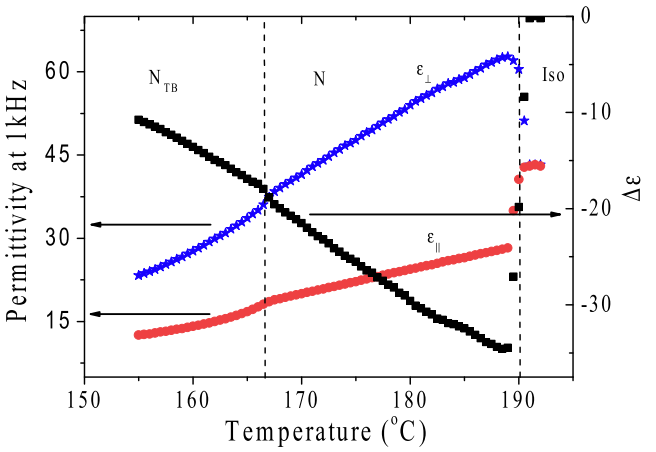

Fig. 9. Plot of the temperature dependence of the real parts of the complex permittivity measured at a frequency of 1 kHz, parallel and perpendicular to the long molecular axis. The calculated dielectric anisotropy Δε (black squares) is plotted versus temperature.

3.5. Dielectric spectroscopy

Dielectric susceptibility χ^* is defined as the ratio of the change in polarization ΔP for a small change in electric field. This is related to complex permittivity ε^* by the equation

$\chi^* \equiv \Delta P/\Delta E = \varepsilon^* - 1$. Measurement of the permittivity is an excellent probe for detecting small changes in helical structures, without alterations, by a weak probe field. Under slow cooling from the Iso state, temperature dependence of the imaginary part of the complex permittivity for planar and homeotropic aligned gold plated cells in the frequency range of 1 Hz to 10 MHz are plotted in Fig. 8a and 8b, respectively. The temperature dependent transverse ($\varepsilon'_{\perp}$) and the longitudinal ($\varepsilon'_{\parallel}$) components of the permittivity deduced for a frequency of 1 kHz are plotted in Fig. 9 as a function of temperature. At the Iso-N transition temperature, the perpendicular component of permittivity $\varepsilon'_{\perp}$ increases sharply whereas the parallel component $\varepsilon'_{\parallel}$ decreases somewhat. After an initial abrupt rise and fall, both the transverse and longitudinal components continually decrease with a reduction in temperature in N and N_{TB} phases. On reaching temperature of the N_{TB}, decrease in both components of the permittivity is accelerated with a reduction in temperature.

3.5.1. Dielectric anisotropy

$\Delta\varepsilon$ is a useful characteristic property of great interest used in designing LC based electro-optic devices. The dielectric anisotropy $\Delta\varepsilon = \left(\varepsilon'_{\parallel} - \varepsilon'_{\perp}\right)$ is found negative for this material for all temperatures. $\Delta\varepsilon$ decreases from 35 at the N-N_{TB} transition temperature to 10 at 12 °C below this phase transition temperature. $\Delta\varepsilon$ for this compound is significantly larger compared to any other compound studied so far, and it also exhibits N_{TB} phase over a broad range of temperatures. A search in the literature shows that the maximum negative dielectric anisotropy for Vertical Alignment (VA) compounds in display applications varies from −3 to −5 [30]. $\Delta\varepsilon$ for a fluoro-based bimesogen compound that exhibits N_{TB} varies from −0.4 to −0.8 [2] and for the cyanobiphenyl bimesogens on the other hand, $\Delta\varepsilon$ varies from + 2 to + 4 [31,32]. In addition, $\Delta\varepsilon$ plays a vital role in determining the field-induced subphases by applying a moderate electric field across a LC cell. The sign of $\Delta\varepsilon$ is dependent on the magnitude and the orientaions of the dipole moments in a molecule. If

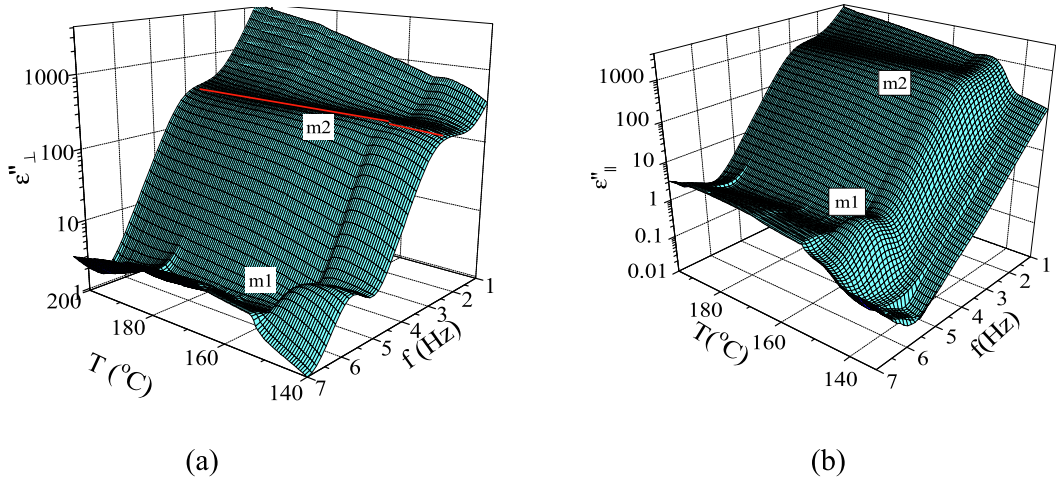

Fig. 8. The three-dimensional (3D) plot of temperature dependent dielectric loss spectra (ε") for (a) 4 μm planar aligned cell and (b) homeotropic gold plated cells in the frequency range 1 Hz – 10 MHz. The temperature is stabilized to within 0.05 °C.

the component of the resultant dipole moment along the long molecular axis is of larger magnitude than normal to it, $\Delta\varepsilon$ is positive and vice versa. For this particular case, the transverse dipole moment component is much larger than the longitudinal one, hence $\Delta\varepsilon$ is negative and significantly large in magnitude.

Depending on the sign of $\Delta\varepsilon$ and on the cell's configuration (planar or homeotropic), molecular director can be realigned by the applied electric field. The reorientation of the molecular director via Freedericksz transition produces a desired change in the optical properties of LC cell, underlying principle of a switching of the pixel in a display. The dc electric field is applied across a homeotropically aligned cell in the N_{TB}, as a result of $\Delta\varepsilon$ being negative, constituent molecules of the compound tilt away from the vertical direction. Textures of homeotropically aligned cell of cell-spacing 4 μm are recorded as the sample cell is cooled slowly from the Iso to mesophases. As the electric field across the cell is increased, molecules tilt and become planarly aligned except closer to the surfaces. The field induced planar textures using POM in the N (Schliern texture at 178 °C, 22 $V_{0\text{-peak}}$ square wave at f = 1.4 kHz) and N_{TB} at (165.7 °C, 76 $V_{0\text{-peak}}$, sine wave at f = 20 kHz) phases are shown in Fig. 10 (Insets in Fig. 10a and 10b correspond to textures in the absence of external field). The focal conic domains in the N_{TB} for T = 165.7 °C (Fig. 10b) are observed close to the N-N_{TB} phase transition temperature.

The measured real and the imaginary parts of the complex permittivity at different temperatures for N and N_{TB} phases of BCI are plotted in Fig. 11. The dielectric spectra reveal two fluctuation modes in the frequency range 1 Hz − 10 MHz. The dielectric relaxation strengths ($\delta\varepsilon$) and the relaxation frequencies (f_t and f_S) of the two modes of the BCI are obtained by fitting the dielectric spectra to Havriliak - Negami empirical equation [33]:

$$\varepsilon^*(\omega) = \varepsilon' - i\varepsilon'' = \varepsilon_\infty + \sum_{j=1}^{n} \frac{\Delta\varepsilon_i}{\left[1 + (i\omega\tau_j)^{\alpha_i}\right]^{\beta_i}} - \frac{i\sigma_{dc}}{\varepsilon_0\omega} \quad (4)$$

ε_∞ is the high frequency permittivity; j = 1 and 2 are the two relaxation processes observed in the experimental frequency window, ε_0 is permittivity of the free space, τ_j is the relaxation time. α_j and β_j are the symmetric and the asymmetric broadening parameters of the j^{th} process. The symmetric distribution parameter $\alpha_{j=1,2} < 1$ is the broadening parameter of the relaxation spectra and a measure of the depression in the Cole-Cole arch. $\alpha = 0$ corresponds to the simple Debye process. $\sigma_{dc}/\varepsilon_0\omega$ is the contribution of dc conductivity to the imaginary part of the permittivity. The relaxation frequency, f_j, of the j^{th} process are related to their τ_j by the equation given in [34].

Frequency dependence of the real and imaginary parts of the complex permittivity for temperatures in N and N_{TB} phases are fitted to equation (4). Amplitudes and frequencies of the two processes are calculated. The BCI exhibits two relaxation processes in N and N_{TB} nematic phases. Temperature dependencies of (a) $\delta\varepsilon_t$ for the high (m_1) and (b) $\delta\varepsilon_s$ for the low (m_2) frequencies corresponding to relaxation frequencies f_t and f_s, are plotted in Fig. 12a and 12b, respectively. The dielectric strength $\delta\varepsilon_t$ for m_1

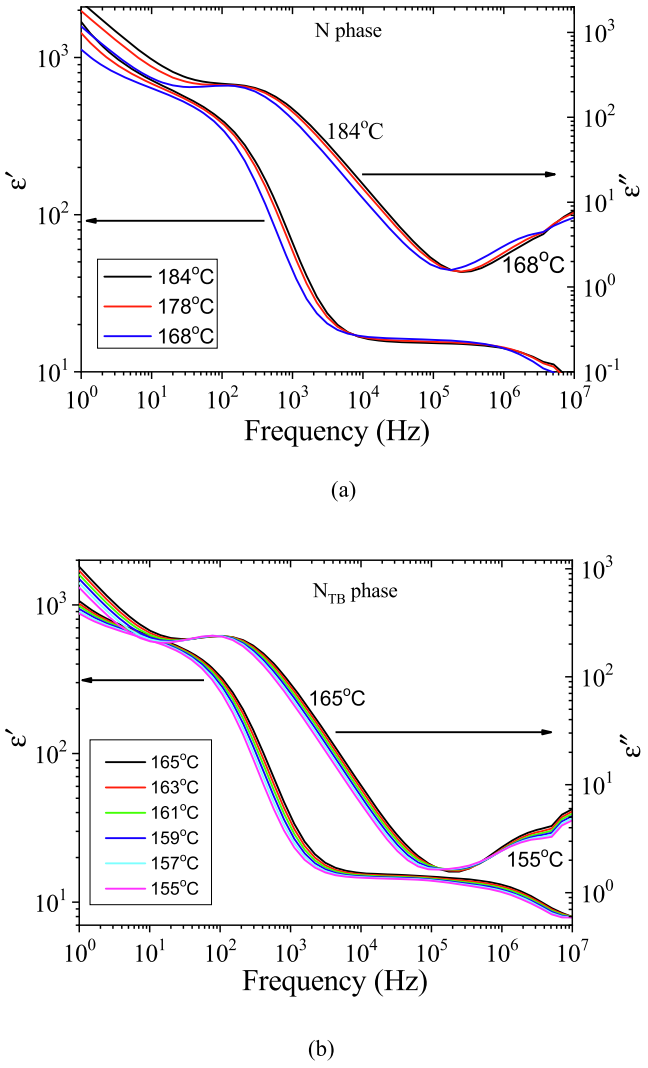

Fig. 11. Permittivity ε' and dielectric loss ε'' of a planar-aligned cell plotted as a function of frequency in (a) N and (b) N_{TB} phases.

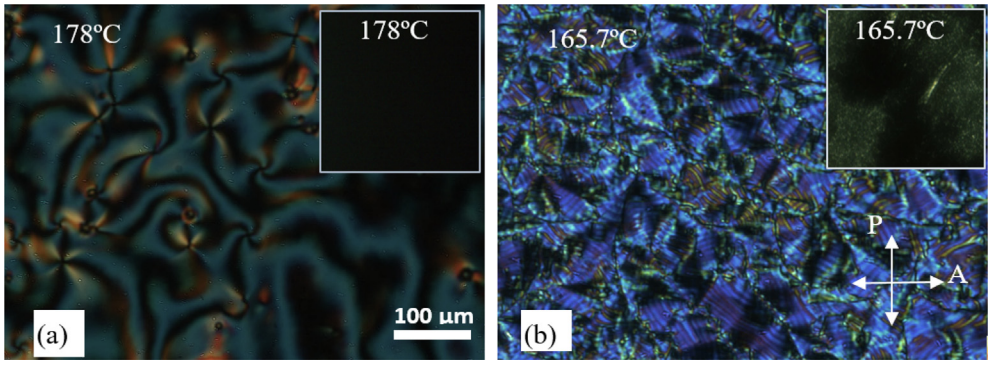

Fig. 10. Microphotographs of 4 μm homeotropic aligned cell with electric field applied across the cell cooled slowly under crossed polarizers: (a) 22 $V_{0\text{-Pk}}$, square wave, f = 1.4 kHz in the N phase at 178 °C and (b) 76 $V_{0\text{-Pk}}$, sine wave, f = 20 kHz. T = 165.7 °C, only 0.3 °C below the N-N_{TB} transition temperature of 166 °C . The Inset in Fig. 10a shows perfect homeotropic alignment in the N phase prior to the external field having been applied and inset in Fig. 10b shows fine networks of focal conic defects in N_{TB} phase recorded by a higher sensitivity camera.

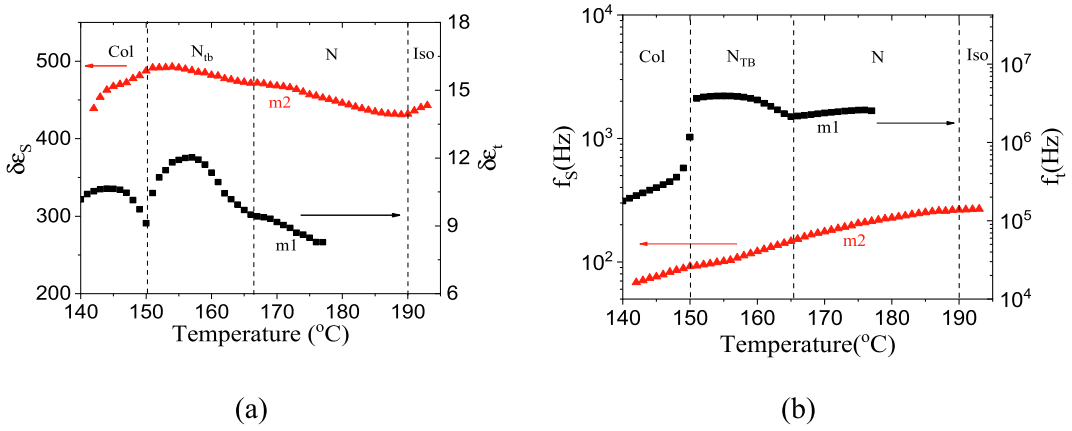

Fig. 12. (a) Plots of the dielectric relaxation strengths, $\delta\varepsilon_t$ and $\delta\varepsilon_s$, and the (b) relaxation frequencies f_t and f_s as functions of temperature for the high (m1) and low frequency modes (m2).

increases at the N-N_{TB} transition temperature, it increases further in the N_{TB} before falling off at N_{TB} to Col phase transition temperature. The relaxation frequency, f_t, of m_1 increases at the N-N_{TB} transition, plateaus within N_{TB} and it then suddenly drops at the N_{TB} to Col transition temperature. The high frequency mode m_1 is assigned to the tilt fluctuations (f_t) of the tilt director without unduly affecting the periodic helical structure of the N_{TB} by a weak probe field.

The high frequency mode behaves anomalously and its frequency softens at the N-N_{TB} transition temperature. This is reminiscent of the presence of soft mode at SmA* and SmC* transition temperature in a ferroelectric liquid crystal. On a reduction in temperature the frequency, f_t , drops down to lower frequencies in the columnar phase. A continual freezing of the structure with a reduction in temperature is reflected here.

A magnified plot of the director tilt fluctuation frequency, f_t, vs. temperature in N and N_{TB} phases is shown in Fig. 13. Here the subscript t refers to the tilt. The plot has striking similarities to those arising from the results of director fluctuations observed in dynamic light scattering experiments of an LC mixture of the dimer with its monomer [35]. Equation for a change in the frequency of the tilt director with temperature is given as follows:

$$2\pi f_t = \frac{1}{\tau_t} = \frac{2K_t q^2 \sin^2\theta}{\gamma} \tag{6}$$

K_t is the elastic constant for the molecular tilt director, γ is the viscosity at the N-N_{TB} transition temperature, and τ_t is the relaxation time of the tilt fluctuations. Results for the tilt mode were obtained independently using a different procedure and agree with those calculated for the viscosity γ = 0.9 Pa•s found for a temperature of 438 K [26]. The low frequency mode is assigned to the hydrodynamic mode $\boldsymbol{q} = q_z\hat{\boldsymbol{z}}$ with the z-dependent rotation of the heloconical director $\hat{\boldsymbol{n}}(\boldsymbol{r})$ and a consequent displacement of the pseudolayers (leading to compression and dilation of the pseudo-layers). This mode persists in the N-phase close to the N-N_{TB} transition temperature, as expected. The wave vector $q = 2\pi/p$, where the pitch in the absence of the external field in N_{TB} phase, $p = p_o$, is ~ 14 nm [18]. γ/q^2 is aproximately a constant, independent of temperature, as due to similar dependencies of q^2 and γ on temperature in numerator and denominator, changes are cancelled out with each other. Hence f_t is related to the heliconical tilt angle θ.

The data for f_t are fitted to eqn. (6) and $K_t sin^2\theta$ deduced from the fit close to the transition temperature are plotted in Fig. 13. Red line is the line of fitting of Eqn (6). If the elastic constant for the molecular tilt K_t is assumed constant close to the N-N_{TB} transition temperature, we find from calculations of θ that the helicoid is spontaneously formed in the N phase close to the transition temperature. The heliconical angle, θ, jumps, at the N- N_{TB} transition followed by a rapid increase in its value with a reduction in temperature, in N_{TB}, as shown in Fig. 14.

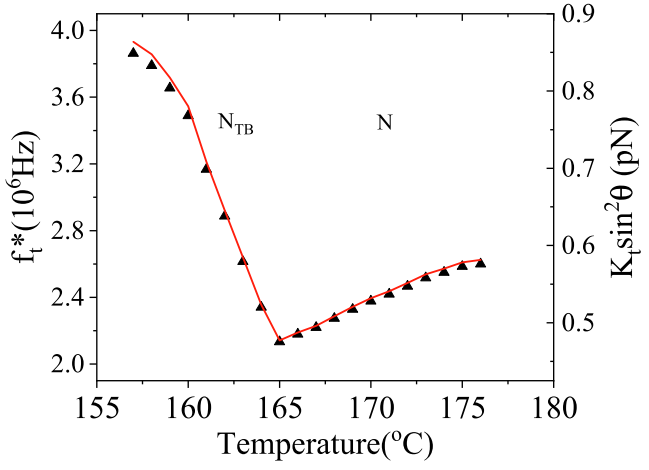

Fig. 13. Temperature dependence of the relaxation frequency of the tilt fluctuation mode (f_t). The red line is the line of fitting to eqn. (6). $K_t sin^2\theta$ values are deduced from the fit close to the transition temperature.

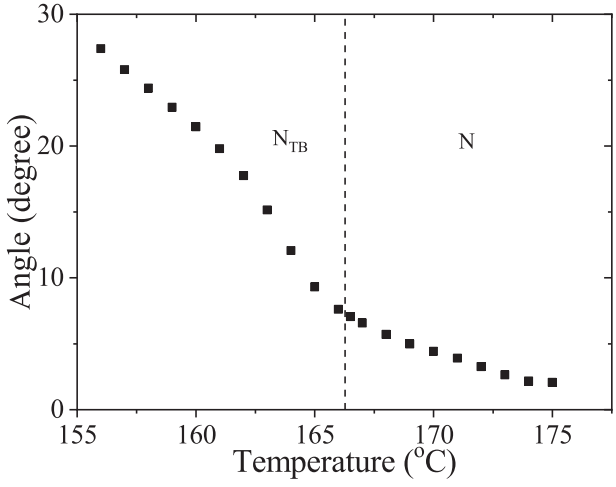

Fig. 14. Variation of the heliconical tilt angle θ as a function of temperature in the N and N_{TB} phases.

The low frequency mode is assigned to the hydrodynamic mode $\boldsymbol{q} = q_z\hat{\boldsymbol{z}}$ with the z-dependent rotation of the heloconical director $\hat{\boldsymbol{n}}(\boldsymbol{r})$, leading to z-dependent displacement of pseudolayers (compression and dilation). This fluctuating mode resembles the symmetry breaking Goldstone mode in ferroelectric liquid crystals. The relaxation time in the low frequency limit is written as [35]:

$$\frac{1}{\tau_S} = 2\pi f_S = \frac{B_e q^2}{2\gamma} \tag{7}$$

B_e is the effective elasticity for the compression of a pseudo layer structure in the N_{TB}. Value of q^2 is found using Eqn. (7). It is assumed that B_e and γ are independent of the electric field. For B_e = 10 pN, q is calculated from p, using $p = 2\pi/q$, the pitch lies in the wavelength range 400 to 800 nm. The three-photon excitation fluorescence polarizing optical microscopy experiment performed in CBC11CB, shown in Fig. 1a, has given q in the sub micrometer range [13]. These observations are confirmed from SEM imaging of the polymerized N_{TB} structure of a mixture of CBC7CB and 5CB [21]. Since this lower frequency mode is found to be of significantly larger dielectric strength, the polar order in N_{TB} is also very large. The bent core mesogen of BCI, though similar in characteristics to the bimesogens (dimers) with odd numbered spacers such as CBC7CB, yet it has different conformational energies. The mesogens are frozen in the columnar structure in two-dimensional ordering as temperature is reduced.

4. Conclusions

From extensive experimental studies carried out on the hockey shaped bent-core liquid crystal, several results are obtained for LC cells in confined conditions of alignment. Using the pyroelectric effect, polarization arising from the flexoelectric effect for a partially unwound helix (as a result of the electric field of 2.2 V/μm applied across a planar aligned cell) in N_{TB} is found 5 nC/cm^2. Such a cell shows large outputs for the first and the second harmonics of the input signal in N_{TB} and N phases, respectively. Result confirm the polar and the chiral characteristic feature of the N_{TB}. From results of the dielectric measurements of the sample in planar and homeotropic aligned cells, $\Delta\varepsilon$ under confined geometrical conditions is calculated at a frequency of 1 kHz for different temperatures. $\Delta\varepsilon$ values are found negative and much larger in magnitude than for compounds studied before. In general a larger $\Delta\varepsilon$ enables an induction of the new field-induced nematic phase/phases for relatively lower electric field strengths. Birefringence measured at a visible wavelength shows a marked reduction in Δn in N and N_{TB} phases relative to those extrapolated from higher to lower temperatures. A reduction in Δn seems to arise from a spontaneous formation of heliconical structure in the N phase close to the N-N_{TB} transition temperature, where helicity continues to persist in the N_{TB} phase. The order parameter, S, shows apparent discontinuity at the I - N and N - N_{TB} transition temperatures. Dielectric measurements in the frequency range 1 Hz to 10 MHz show two collective modes. The higher frequency mode is assigned to the tilt fluctuations of the heliconical angle in the N and N_{TB} phases with strong temperature dependencies of the frequencies recorded. This shows softening of the relevant frequency at the N to N_{TB} transition similar to that observed for SmA-SmC* transition temperature. However the lower frequency mode is significantly larger in strength and is assigned to the compression and dilation of the periodic pseudo-layer structure of the phase. On cooling the sample from the Iso state, the heliconical angle increases with a reduction in temperature, it jumps at the N-N_{TB} transition temperature and continues to increase with a further reduction in temperature. Temperature dependence of the heliconical angle accords with the Landau model [36]. It has been argued that the structure of the N_{TB} phase is a result of efficiency of the molecular packing arising from shape entropy of the constituent molecules [37]. Recently a set of molecules (CB6O.m, m < 10, m is the number of methylene units in the spacer), similar in structure to the trimer already discussed [7], have exhibited N_{TB} over a restricted range of temperatures [38].

Declaration of Competing Interest

The authors declare that they have no known competing financial interests or personal relationships that could have appeared to influence the work reported in this paper.

Funding and Acknowledgement

Work was supported by the US-Ireland program, grant 13/US/I12866, jointly administered with the National Science Foundation USA (grant number NSF-DMR-1410649). One of the authors (NY) thanks the Irish Research Council for awarding the Government of Ireland Postdoctoral Fellowship 2021, GOIPD/2021/858. G Shanker, sincerely thanks Bangalore University Jnana Bharathi Campus, Bengaluru-560056 with UNI.ORDER.No. DEV:D2a:BU-RP: 2020-21 for financial support. The authors also thank Dr. Vitaly P. Panov for discussions.

References

[1] V.P. Panov, M. Nagaraj, J.K. Vij, Y.P. Panarin, A. Kohlmeier, M.G. Tamba, R.A. Lewis, G.H. Mehl, Spontaneous Periodic Deformations in Nonchiral Planar-Aligned Bimesogens with a Nematic-Nematic Transition and a Negative Elastic Constant, Phys. Rev. Lett. 105 (2010), https://doi.org/10.1103/Phys. Rev. Lett. 105.167801 167801.
[2] V. Borshch, Y.-K. Kim, J. Xiang, M. Gao, A. Jákli, V.P. Panov, J.K. Vij, C.T. Imrie, M. G. Tamba, G.H. Mehl, O.D. Lavrentovich, Nematic twist-bend phase with nanoscale modulation of molecular orientation, Nat. Commun. 4 (2013) 2635, https://doi.org/10.1038/ncomms3635.
[3] D. Chen, J.H. Porada, J.B. Hooper, A. Klittnick, Y. Shen, M.R. Tuchband, E. Korblova, D. Bedrov, D.M. Walba, M.A. Glaser, J.E. Maclennan, N.A. Clark, Chiral heliconical ground state of nanoscale pitch in a nematic liquid crystal of achiral molecular dimers, Proc. Natl. Acad. Sci. USA. 110 (40) (2013) 15931–15936, https://doi.org/10.1073/pnas.1314654110.
[4] R. B. Meyer, Structural problems in liquid crystal physics. In: Balian R, Weil G, editors. Les Houches summer school in theoretical physics, 1973. Molecular fluids. New York (NY): Gordon and Breach; 1976. 273–373.
[5] I. Dozov, On the spontaneous symmetry breaking in the mesophases of achiral banana-shaped molecules, Europhys. Lett. 56 (2) (2001) 247–253, https://doi.org/10.1209/epl/i2001-00513-x.
[6] R. Memmer, Liquid crystal phases of achiral banana-shaped molecule, Liq. Cryst. 29 (2002) 483–496, https://doi.org/10.1080/02678290110104586.
[7] Y. Wang, G. Singh, D.M. Agra-Kooijman, M. Gao, H.K. Bisoyi, C. Xue, M.R. Fisch, S. Kumar, Q. Li, Room temperature heliconical twist-bend nematic liquid crystal, Cryst. Eng. Comm. 17 (2015) 2778–2782, https://doi.org/10.1039/C4CE02502D.
[8] V.P. Panov, R. Balachandran, M. Nagaraj, J.K. Vij, M.G. Tamba, A. Kohlmeier, G.H. Mehl, Microsecond linear optical response in the unusual nematic phase of achiral bimesogens, Appl. Phys. Lett. 99 (2011), https://doi.org/10.1063/1.3671996 261903.
[9] V.P. Panov, R. Balachandran, J.K. Vij, M.G. Tamba, A. Kohlmeier, G.H. Mehl, Field-induced periodic chiral pattern in the Nx phase of achiral bimesogens, Appl. Phys. Lett. 101 (2012), https://doi.org/10.1063/1.4769458 234106.
[10] L. Beguin, J.W. Emsley, M. Lelli, A. Lesage, G.R. Luckhurst, B.A. Timimi, H. Zimmermann, The chirality of a twist-bend nematic phase identified by NMR spectroscopy, J. Phys. Chem. B 116 (27) (2012) 7940–7951, https://doi.org/10.1021/jp302705n.
[11] C. Zhu, M.R. Tuchband, A. Young, M. Shuai, A. Scarbrough, D.M. Walba, J.E. Maclennan, C. Wang, A. Hexemer, N.A. Clark, Resonant Carbon K-Edge Soft X-Ray Scattering from Lattice-Free Heliconical Molecular Ordering: Soft Dilative Elasticity of the Twist-Bend Liquid Crystal Phase, Phys. Rev. Lett. 116 (2016), https://doi.org/10.1103/PhysRevLett.116.147803 147803.
[12] W.D. Stevenson, Z. Ahmed, X.B. Zeng, C. Welch, G. Ungar, G.H. Mehl, Molecular organization in the twist-bend nematic phase by resonant X-ray scattering at the Se K-edge and by SAXS, WAXS and GIXRD, Phys. Chem. Chem. Phys. 19 (21) (2017) 13449–13454, https://doi.org/10.1039/C7CP01404J.
[13] V.P. Panov, M.C.M. Varney, I.I. Smalyukh, J.K. Vij, M.G. Tamba, G.H. Mehl, Hierarchy of periodic patterns in the Twist-bend nematic phase of mesogenic dimers, Mol. Cryst. Liq. Cryst. 611 (2015) 180–185, https://doi.org/10.1080/15421406.2015.1030.252.

[14] V.P. Panov, J.K. Song, G.H. Mehl, J.K. Vij, The beauty of twist-bend nematic phase: Fast switching Domains, First Order Freedericksz transition and a hierarchy of structures, Crystals 11 (2021) 621–643, https://doi.org/10.3390/cryst11060621.
[15] S.P. Sreenilayam, V.P. Panov, J.K. Vij, S. Shanker, The N_{TB} phase in an achiral asymmetrical bent-core liquid crystal terminated with symmetric alkyl chains, Liq. Cryst. 44 (2017) 244–253, https://doi.org/10.1080/02678292.2016.1253878.
[16] I. Haller, Thermodynamic and static properties of liquid crystals, Prog. Solid State Chem. 10 (1975) 103–118, https://doi.org/10.1016/0079-6786 (75) 90008-4.
[17] M.W. Schröder, S. Diele, G. Pelzl, U. Dunemann, H. Kresse, W. Weissflog, Different nematic phases and a switchable SmCP phase formed by homologues of a new class of asymmetric bent-core mesogens, J. Mater. Chem. 13 (8) (2003) 1877–1882, https://doi.org/10.1039/b305451a.
[18] D. Chen, M. Nakata, R. Shao, M.R. Tuchband, M. Shuai, U. Baumeister, W. Weissflog, D.M. Walba, M.A. Glaser, J.E. Maclennan, N.A. Clark, Twist-bend heliconical chiral nematic liquid crystal phase of an achiral rigid bent-core mesogen, Phys. Rev. E. 89 (2014) 0225067, https://doi.org/10.1103/PhysRevE.89.022506.
[19] V. P. Panov, J. K. Vij, R. Balachandran, V. Borsch, O.D. Lavrentovich, M. G. Tamba and G. H. Mehl. Properties of the self-deforming Ntb phase in mesogenic dimers, Proc. SPIE 8828, Liquid Crystals XVII (2013) 88280X, doi: 10.1117/12.2024470
[20] D.M. Agra Kooijman, G. Singh, M.R. Fisch, M.R. Vangatesan, J.-K. Song, S. Kumar, The oblique chiral nematic phase in calamitic bimesogens, Liq. Cryst. 44 (2017) 191–203, https://doi.org/10.1080/02678292.2016.1272141.
[21] V.P. Panov, S.P. Sreenilayam, Y.P. Panarin, J.K. Vij, C. Welch, G.H. Mehl, Characterization of the Submicrometer Hierarchy Levels in the Twist-Bend Nematic Phase with Nanometric Helices via Photopolymerization. Explanation for the Sign Reversal in the Polar Response, Nano. Lett. 17 (2017) 7515–7519, https://doi.org/10.1021/acs.nanolett.7b03441.
[22] K. Miyasato, S. Abe, H. Takezoe, A. Fukuda, E. Kuze, Direct method with triangular waves for measuring spontaneous polarization, Jap. J. Appl. Phys. 22 (1983) L661, https://doi.org/10.1143/JJAP.22.L661.
[23] V. M. Vaksman and Y. P. Panarin, Measurement of Ferroelectric Liquid Crystal Parameters. Mol. Mat. 1 (1992) 147-154, doi:10.21427/D7FF8R ; V. P. Panov, J. K. Vij and N. M. Shtykov, A field reversal method for measuring parameters of a ferroelectric liquid crystal, Liq. Cryst. 28 (2001) 615-620, doi:10.1080/02678290010020175
[24] A. Kocot, R. Wrzalik, J.K. Vij, R. Zentel, Pyroelectric and electro-optic effects in SmC* phase of a polysiloxane ferroelectric liquid crystal, J. Appl. Phys. 75 (1994) 728–733, https://doi.org/10.1063/1.356986.
[25] R Balachandran, V.P. Panov, Y.P. Panarin, J.K. Vij, M.G. Tamba, G.H. Mehl, J.K. Song, Flexoelectric behavior of bimesogenic liquid crystals in the nematic phase – observation of a new self-assembly pattern at the twist-bend nematic and the nematic interface, J. Mater. Chem. C 2 (2014) 8179–8184, https://doi.org/10.1039/c4tc01043d.
[26] K. Merkel, A. Kocot, J.K. Vij, G. Shanker, Distortions in structures of the twist bend nematic phase of a bent-core liquid crystal by the electric field, Phys. Rev. E 98 (2018) 022704, https://doi.org/10.1103/Phys Rev. E.98.022704.
[27] C. Meyer, C. Blanc, G.R. Luckhurst, P. Davidson, I. Dozov, Biaxiality-driven twist-bend to splay-bend nematic phase transition induced by an electric field, Sci. Adv. 6 (2020) eabb8212–1-11, https://doi.org/10.1126/sciadv.abb8212.
[28] O.E. Panarina, Y.P. Panarin, F. Antonelli, J.K. Vij, M. Reihmann, G. Galli, Investigation of de Vries SmA* mesophases in low molecular weight organosiloxane compounds, J. Mater. Chem. 16 (2006) 842–849, https://doi.org/10.1039/b509119e.
[29] Z. Zhang, V.P. Panov, M. Nagaraj, R.J. Mandle, J.W. Goodby, G.R. Luckhurst, J.C. Jones, H.F. Gleeson, Raman scattering studies of order parameters in liquid crystalline dimers exhibiting the nematic and twist-bend nematic phases, J. Mater. Chem. C 3 (2015) 10007–10016, https://doi.org/10.1039/c5tc02174j.
[30] Y. Chen, F. Peng, T. Yamaguchi, X. Song, S.-T. Wu, High performance negative dielectric anisotropy liquid crystals for display applications, Crystals 3 (2013) 483–503, https://doi.org/10.3390/cryst3030483.
[31] R. Balachandaran, V.P. Panov, J.K. Vij, A. Kocot, M.G. Tamba, A. Kohlmeier, G.H. Mehl, Elastic properties of bimesogenic liquid crystals, Liq. Cryst. 40 (2013) 681–688, https://doi.org/10.1080/02678292.2013.765973.
[32] C.-J. Yun, M.R. Vengatesan, J.K. Vij, J.-K. Song, Hierarchical elasticity of bimesogenic liquid crystals with twist-bend nematic phase, Appl. Phys. Lett. 106 (2015), https://doi.org/10.1063/1.4919065 173102.
[33] S. Havriliak, S. Negami, A complex plane representation of dielectric and mechanical relaxation processes in polymers, Polymer 8 (1967) 161–210, https://doi.org/10.1016/0032-3861(67)90021-3.
[34] O.E. Kalinovskava, J.K. Vij, The exponential dielectric relaxation dynamics in a secondary alcohol's supercooled liquid and glassy states, J. Chem. Phys. 112 (2000) 3262–3266, https://doi.org/10.1063/1.480909.
[35] Z. Parsouzi, S.M. Shamid, V. Borshch, P.K. Challa, A.R. Baldwin, M.G. Tamba, C. Welch, G.H. Mehl, J.T. Gleeson, A. Jakli, O.D. Lavrentovich, D.W. Allender, J.V. Selinger, S. Sprunt, Fluctuation Modes of a Twist-Bend Nematic Liquid Crystal, Phys. Rev. X 6 (2016), https://doi.org/10.1103/PhysRevX.6.021041 021041.
[36] C. Meyer, G.R. Luckhurst, I. Dozov, The temperature dependence of the heliconical tilt angle in the twist-bend nematic phase of the odd dimer CB7CB, J. Mater. Chem. C 3 (2015) 318–328, https://doi.org/10.1039/C4TC01927J.
[37] J.W. Goodby, Nano-objects-sculpting and shape in molecular material design (The P.G. deGennes ILCS prize lecture), Liq. Cryst. 46 (2019) 1901–1924, https://doi.org/10.1080/02678292.2019.1643508.
[38] D. Pociecha, N. Vaupotic, M. Majeswska, E. Cruickshank, R. Walker, J.M.D. Storey, C.T. Imrie, C. Wang, E. Gorecka, Photonic Bandgap in Achiral Liquid Crystals—A Twist on a Twist, Adv. Mater. 33 (2021), https://doi.org/10.1002/adma.202103288 2103288.